

EVOLUTION OF ERUPTIVE FLARES. II. THE OCCURRENCE OF LOCALLY ENHANCED RESISTIVITY

TETSUYA MAGARA¹ AND KAZUNARI SHIBATA²

Received 1998 June 8; accepted 1998 October 20

ABSTRACT

In this paper we study resistive processes in the preflare phase of eruptive flares by means of the 2.5-dimensional MHD numerical simulation. According to many detailed observations of solar flares, their evolution is characterized by several phases, each of which has a distinct nature. In the first phase, some kinds of radiation begin to be enhanced gradually, which implies the occurrence of the preflare heating. Then, at a certain time, that gradual energy-release phase is replaced by the violent energy-release phase in which a huge amount of energy is released in various forms. So far, the nature of this violent energy-release phase has been well studied by using a flare model based on the fast magnetic reconnection, although those problems of the preflare heating and the transition from the gradual energy-release phase to the violent one have not been sufficiently discussed yet. In this paper, in order to tackle these problems, we start with a 2.5-dimensional force-free current sheet under a uniformly distributed resistivity, which is subject to a very small random velocity perturbation. At first the evolution enters on the linear stage of tearing instability and later a sufficient amount of thermal energy is produced in the nonlinear stage, which is considered to have a relation with the preflare heating. In this nonlinear stage, the component of magnetic fields perpendicular to the sheet (perpendicular magnetic fields) flows away from X-points formed in the sheet and eventually the *current sheet collapses* at these points. This collapse strongly reduces the thickness of the sheet if the magnetic Reynolds number is quite large and the plasma beta is quite low. Since the formation of thin current sheet leads to the occurrence of locally enhanced resistivity (anomalous resistivity), the transition from the gradual energy-release phase under a uniformly distributed resistivity to the violent one under a locally enhanced anomalous resistivity can be accomplished, which causes the fast magnetic reconnection responsible for various explosive phenomena in the Sun.

Subject headings: MHD — Sun: corona — Sun: flares — Sun: magnetic fields

1. INTRODUCTION

Explosive phenomena are often observed in the solar corona, which are now widely believed to be energy conversion processes from the magnetic energy to the other types of energy. Since the corona is generally a good conductive medium, any dynamical evolution in the corona is usually described within the context of ideal MHD theory, where the effect of resistivity is negligible. It is therefore necessary to investigate the small-scale region where the magnetic energy can be efficiently converted into the other types of energy when we consider any explosive phenomenon in the corona. That region in which a certain component of magnetic fields changes abruptly across the sheet so that a large amount of currents can flow through it is known as current sheet. Owing to this enhancement of current density, the Ohmic dissipation efficiently works in current sheet, compared with other normal regions in the corona.

From this viewpoint, many authors have tried to explain various coronal explosive phenomena by using the concept of current sheet. For example, Heyvaerts, Priest, & Rust (1977) presented a flare model, in which a current sheet was formed between the emerging subphotospheric magnetic field and the overlying coronal magnetic field. This flare model was lately investigated in detail by Shibata et al. (1989, 1992) and Yokoyama & Shibata (1996) who performed two-dimensional MHD numerical simulations and

clarified many interesting features of this type of flares. As for the model of the so-called two-ribbon flares, Mikic, Barnes, & Schnack (1988), Biskamp & Welter (1989), Finn, Guzdar, & Chen (1992), Inhester, Birn, & Hesse (1992), Kusano et al. (1994), Choe & Lee (1996), and Amari et al. (1996) succeeded to develop a model in which a current sheet is formed within a magnetic arcade by imposing a particular photospheric motion in either the single-arcade or the multiple-arcade system. Forbes & Priest (1983), Forbes, Malherbe, & Priest (1989), and Forbes & Malherbe (1991) performed two-dimensional MHD numerical simulations in order to study the physical structure of the two-ribbon flares. They found that a closed magnetic structure was formed in the lower part of a current sheet and that structure well reproduced several observational features of postflare loops. With respect to the coronal heating, Parker (1994) discussed that current sheets were spontaneously formed as singular layers in the corona where a sufficient amount of thermal energy for the coronal heating is produced by the Ohmic dissipation. Recently, Karpen, Antiochos, & DeVore (1996) showed an interesting simulation result that many current sheets are distributed all over an active region.

When we study the natures of solar flares, we have an important problem with their timescale. Since the magnetic Reynolds number in the corona is quite large, diffusive processes in current sheet proceed very slowly, which cannot explain such a short timescale as is observed in real flares. This problem has prompted solar physicists to consider a rapid energy-conversion mechanism in the current sheet,

¹ Hida Observatory, Faculty of Science, Kyoto University, Kamitakara, Gifu 506, Japan; magara@kusastro.kyoto-u.ac.jp.

² National Astronomical Observatory, Mitaka, Tokyo 181, Japan.

which is now known as magnetic reconnection. Historically, the Sweet-Parker model (Sweet 1958; Parker 1963) was the first dynamical model and later Petschek (1964) proposed a remarkable model in which the rate of magnetic reconnection was little dependent on the magnetic Reynolds number. The main difference between these two models lies in the size of a diffusion region. The Sweet-Parker model has a long diffusion region while the Petschek model has a small one, which makes the latter a more efficient energy converter than the former.

Petschek's proposal seemed to solve the problem of the timescale of solar flares, although there appeared one big difficulty in forming a small diffusion region. Biskamp (1986) performed two-dimensional MHD numerical simulations under a uniformly distributed resistivity and showed that a diffusion region became longer as the magnetic Reynolds number is large. This implies that the Petschek's configuration does not arise but Sweet-Parker's does in such a large magnetic-Reynolds-number system as the solar corona (see Biskamp 1993 for details).

On the other hand, by assuming a localized resistivity in current sheet, Ugai & Tsuda (1977) and Sato & Hayashi (1979) successfully reproduced the Petschek-like configuration in their two-dimensional MHD numerical simulations. Ugai regarded the localization of resistivity as a key factor in the efficient energy-conversion mechanism and then developed the fast-magnetic-reconnection model, in which a locally enhanced anomalous resistivity naturally brings about such a converging flow pattern as is preferred by the Petschek model. (In this respect, Priest & Forbes 1986 and Priest 1991 claimed that the nature of magnetic reconnection was characterized by the flow pattern seen in the system, although this has not yet been confirmed by self-consistent MHD simulations.) Ugai's recent researches in the fast magnetic reconnection can be seen in Ugai (1994, 1995) and Ugai & Shimizu (1996).

By using a flare model based on the fast magnetic reconnection, Magara et al. (1996) and Magara, Shibata, & Yokoyama (1997) studied natures of eruptive flares and succeeded to explain several new observational results obtained by *Yohkoh*. However, as Magara et al. (1997) mentioned, there remains one problem about the initial localization of resistivity which later causes the violent energy release. In Magara et al. (1996, 1997), that initial localization of resistivity was given by a particularly selected perturbation. However, in actual situations, that localization does not occur independently but it occurs through the mutual interaction among several physical processes of the flare evolution. Therefore, in order to understand the overall evolution of solar flares, we need to clarify how the localization of resistivity proceeds in the flare evolution (see Shibata 1997). The aim of this paper is to study this problem by paying a particular attention to the nonlinear resistive evolution of current sheet.

The next section presents the basic description of this study. In §§ 3 and 4, we exhibit and discuss our results. Our conclusion and summary are given in §§ 5 and 6, respectively.

2. BASIC FORMULATION

2.1. Basic Equations

In this study, we use the standard set of MHD equations, except that the effects of gravity and viscosity are both

neglected. These equations are expressed as follows:

$$\frac{\partial \rho}{\partial t} + \nabla \cdot (\rho \mathbf{v}) = 0, \quad (1)$$

$$\rho \left[\frac{\partial \mathbf{v}}{\partial t} + (\mathbf{v} \cdot \nabla) \mathbf{v} \right] = -\nabla P + \frac{1}{4\pi} (\nabla \times \mathbf{B}) \times \mathbf{B}, \quad (2)$$

$$\frac{\rho^\gamma}{\gamma - 1} \left[\frac{\partial}{\partial t} \left(\frac{P}{\rho^\gamma} \right) + (\mathbf{v} \cdot \nabla) \left(\frac{P}{\rho^\gamma} \right) \right] = \frac{\eta}{4\pi} |\nabla \times \mathbf{B}|^2, \quad (3)$$

$$\frac{\partial \mathbf{B}}{\partial t} = \nabla \times (\mathbf{v} \times \mathbf{B}) - \nabla \times (\eta \nabla \times \mathbf{B}), \quad (4)$$

$$P = \frac{\rho R T}{\mu}, \quad (5)$$

where ρ , \mathbf{v} , \mathbf{B} , P , γ , η , μ , R , and T mean the gas density, flow velocity, magnetic field, gas pressure, adiabatic index, magnetic diffusivity, mean molecular weight, gas constant, and temperature, respectively. On the basis of these equations, we perform the 2.5-dimensional MHD numerical simulation in the Cartesian coordinate. All the physical variables are dependent on both the x -coordinate and the z -coordinate but independent of the y -coordinate, while the y -components of velocity and magnetic fields are included in our calculations, which means the 2.5-dimensional numerical simulation. In practice, all the calculations are carried out in the nondimensional form based on several physical units summarized in Table 1.

2.2. Initial Conditions and Boundary Conditions

Figure 1 shows the initial conditions of our numerical simulation. Since the aim of our study is to investigate the dynamical behavior of the current sheet formed in the corona, we assume that the sheet is initially in a force-free state, in which both the antiparallel component (z -component) and the perpendicular component (y -component) of magnetic fields exist. Accordingly, the initial distributions of physical variables are expressed as

$$B_x = 0, \quad (6)$$

$$B_y = \frac{B_0}{\cosh(4\pi x/L)}, \quad (7)$$

$$B_z = -B_0 \tanh\left(4\pi \frac{x}{L}\right), \quad (8)$$

$$P = P_0, \quad (9)$$

$$\rho = \rho_0, \quad (10)$$

and

$$T = T_0, \quad (11)$$

where $P_0 = 1/\gamma$, $B_0 = (8\pi P_0/\beta)^{1/2}$, $T_0 = \gamma P_0/\rho_0$. Here β is the so-called plasma beta (the ratio of gas pressure to magnetic pressure), and in this study we usually set $\gamma = 5/3$, $\beta = 0.15$, and $\rho_0 = 1$ except for the high- β case ($\beta = 0.2$) and the low- β case ($\beta = 0.1$).

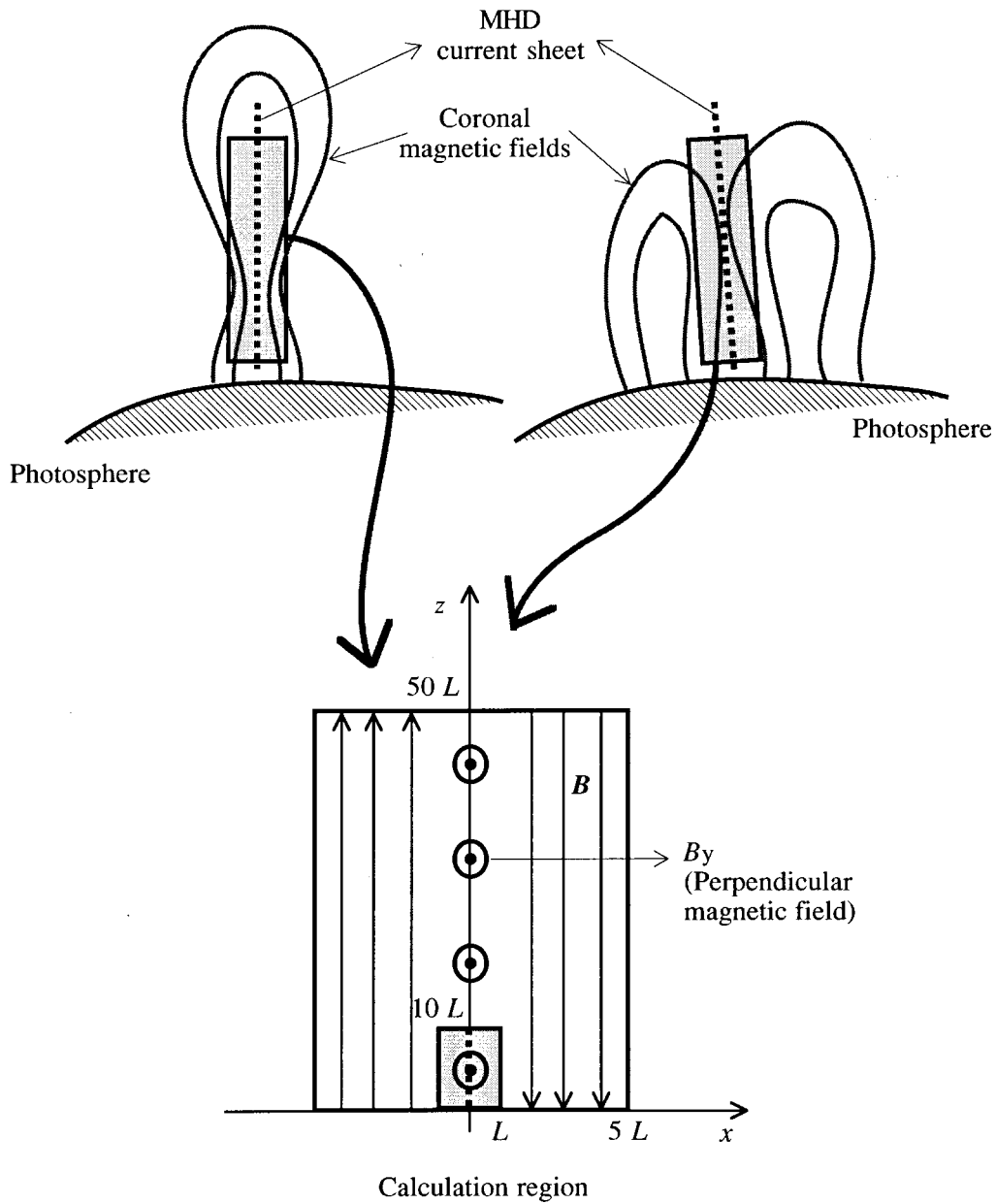


FIG. 1.—Calculation region and initial conditions of our numerical simulation are displayed, associated with some examples of the current sheet formed in the corona. A gray area indicates the region of fine meshes.

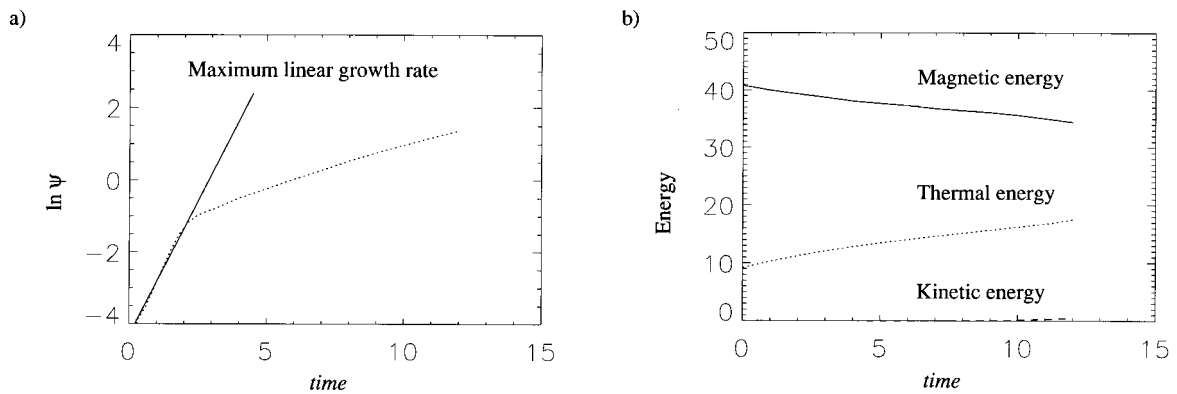


FIG. 2.—(a) Time variation of the logarithmic increment of the reconnected magnetic flux $\psi(t)$ (dotted line) produced on the part of the z -axis, $0 \leq z \leq 10$, in the standard case ($\beta = 0.15$ and $R_m = 1000$). An evolutionary line of the maximum linear growth rate of tearing instability is also shown by a solid line. (b) Time variations of the magnetic energy $E_m(t)$ (solid line), thermal energy $E_{th}(t)$ (dotted line), and kinetic energy $E_k(t)$ (broken line) in the standard case ($\beta = 0.15$ and $R_m = 1000$).

As for the actual calculations, we use the modified Lax-Wendroff scheme and carry out our calculations only over a half-domain ($0 \leq x \leq 5L$, $0 \leq z \leq 50L$) of the calculation region shown in Figure 1 by assuming a symmetry with respect to the z -axis. In addition, the calculation region is divided into three areas, each of which has fine meshes, intermediate ones, and coarse ones. The fine-mesh area ($-L \leq x \leq L$, $0 \leq z \leq 10L$) has the mesh size of $(\Delta x, \Delta z) = (0.004L, 0.04L)$ and this area is displayed in gray in Figure 1. The coarse-mesh area has the mesh size of $(\Delta x, \Delta z) = (0.1L, 1.0L)$, located near the boundary of the calculation region. Consequently, the total mesh number is $(N_x \times N_z) = (340 \times 340)$. As is derived in equation (8), the total thickness of the sheet is initially about $L/2\pi$ so that the initial number of grid points included inside the sheet is about 40.

The boundary conditions are described as follows. As both the top boundary (at $z = 50L$) and the bottom boundary (as $z = 0$), we set

$$\frac{\partial \rho}{\partial z} = \frac{\partial v_x}{\partial z} = v_y = v_z = B_x = \frac{\partial B_y}{\partial z} = \frac{\partial B_z}{\partial z} = \frac{\partial P}{\partial z} = 0. \quad (12)$$

On the z -axis (at $x = 0$), we set

$$\frac{\partial \rho}{\partial x} = v_x = v_y = \frac{\partial v_z}{\partial x} = \frac{\partial B_x}{\partial x} = \frac{\partial B_y}{\partial x} = B_z = \frac{\partial P}{\partial x} = 0. \quad (13)$$

At the side boundary (at $x = 5L$), we set

$$\frac{\partial \rho}{\partial x} = v_x = v_y = \frac{\partial v_z}{\partial x} = B_x = \frac{\partial B_y}{\partial x} = \frac{\partial B_z}{\partial x} = \frac{\partial P}{\partial x} = 0. \quad (14)$$

2.3. Initial Perturbation

Magara et al. (1996, 1997) used a model based on the fast magnetic reconnection and succeeded to reproduce several violent natures of eruptive flares. In these previous works we regarded the state of locally enhanced resistivity as the initial state of simulations, although, in the present work, this state is not the initial state. The locally enhanced resistivity results from the occurrence of anomalous resistivity, which requires a very thin current sheet, that is, the thickness of the sheet must lie in the range of microscopic values. In the active region of the solar corona, this value is thought to be about 10 m. [For example, Priest 1982 shows the condition of the thickness as $l_0 < 1.3 \times 10^{13} B_0 / (nT^{1/2})$ cm, with B_0 in G, n in cm^{-3} , and T in K. Hence the critical length becomes 13 m when $T = 10^6$ K, $n = 10^9 \text{ cm}^{-3}$, and $B_0 = 10^2$ G.] As to the formation of current sheets in the corona, many authors have studied and confirmed that an MHD current sheet, whose length and thickness are still in the range of macroscopic values, was formed within a magnetic arcade through ideal MHD thinning processes (Mikic et al. 1988; Biskamp & Welter 1989; Finn et al. 1992; Inhester et al. 1992; Kusano et al. 1994; Choe & Lee 1996; Amari et al. 1996). The next step is to determine how the thickness of the current sheet falls in the range of microscopic values, which can cause the anomalous resistivity. In this respect, it is unrealistic to imagine that the thickness of the sheet is reduced from the range of macroscopic values (10 km, for example) toward the range of microscopic values (10 m, for example) only through ideal MHD thinning processes,

because the resistive processes based on a large magnetic Reynolds number in the corona probably work before the thickness of the sheet falls in the range of microscopic values. In other words, the timescale of resistive processes eventually become shorter than that of the ideal MHD thinning processes. From these considerations, it seems reasonable that we start with an MHD current sheet of macroscopic thickness, which is subject to the diffusive effect caused by not a locally enhanced but a uniformly distributed resistivity.

Accordingly, we initially assign a uniformly distributed resistivity. In addition, we impose a very small random velocity perturbation within the region of $(-0.08L, 2L) \leq (x, z) \leq (0.08L, 8L)$ as the initial perturbation. Owing to the limitation of our numerical simulation, the magnetic Reynolds number, $R_m (\equiv c_s L/\eta)$, is mainly set to be $R_m = 1000$ and the maximum amplitude of the random velocity perturbation is set to be less than 1% of v_A , where $c_s [\equiv (\gamma P_0/\rho_0)^{1/2}]$ and $v_A [\equiv B_0/(4\pi\rho_0)^{1/2}]$ are the adiabatic sound velocity and the Alfvén velocity in the initial state.

3. LINEAR AND NONLINEAR EVOLUTION OF TEARING INSTABILITY IN A UNIFORMLY DISTRIBUTED RESISTIVITY

3.1. Growth Rate and Energetics

In this section, we show several basic features observed in our numerical simulation by using the results of the standard case ($\beta = 0.15$, $R_m = 1000$).

Figure 2a represents the time variation of the logarithmic increment of the reconnected magnetic flux ψ produced on the part of the z -axis (*dotted line*), which is defined as

$$\psi(t) = \int_0^{10} |B_x(0, z, t)| dz. \quad (15)$$

This value is often used as an evolutionary index for the tearing process in current sheet. According to the precise linear analysis (see Furth, Killeen, & Rosenbluth 1963; Sturrock 1994), the maximum growth rate in the linear stage of this process is given by $\gamma_m \sim 0.63[\tau_d \tau_A]^{-1/2}$, where τ_d and τ_A mean the diffusion time and the Alfvén crossing time, both of which are defined as

$$\tau_d = \frac{l^2}{\eta}, \quad (16)$$

and

$$\tau_A = \frac{l}{v_A}, \quad (17)$$

where l is a half-thickness of the current sheet. In our formulation, the unit of time is given by the sound crossing time, $\tau_s (\equiv L/c_s)$, so that

$$\frac{\tau_d}{\tau_s} = \frac{l^2/\eta}{L/c_s} = \frac{c_s L}{\eta} \left[\frac{l}{L} \right]^2 = R_m \left[\frac{l}{L} \right]^2, \quad (18)$$

$$\frac{\tau_A}{\tau_s} = \frac{c_s}{v_A} = \frac{c_s}{v_A} \frac{l}{L} = \left[\frac{\gamma\beta}{2} \right]^{1/2} \frac{l}{L}. \quad (19)$$

Hence we obtain the normalized growth rate as $\gamma_m \tau_s \sim 0.63 R_m^{1/2} [\gamma\beta/2]^{1/4} [l/L]^{3/2}$. This is about 1.49 with $R_m = 1000$, $\gamma = 5/3$, $\beta = 0.15$, and $l/L = (4\pi)^{-1}$. In Figure 2a, we also draw the evolutionary line of this growth rate, represented by a solid line.

TABLE 1
UNITS FOR NORMALIZATION

Physical Values	Normalization Units
Length	L
Velocity	c_s^a
Time	L/c_s
Density	ρ_0
Pressure	$\rho_0 c_s^2$
Temperature	$\mu c_s^2/\gamma R$
Magnetic field	$(8\pi\rho_0 c_s^2/\gamma\beta_0)^{1/2}$
Magnetic diffusivity	$c_s L$

NOTE— γ , μ , β_0 , and R are the adiabatic index, the mean molecular weight, the plasma beta, and the gas constant, respectively.

^a c_s is the adiabatic sound velocity defined by $c_{s0} \equiv (\gamma RT_0/\mu)^{1/2}$.

In Figure 2b, the time variations of the magnetic energy E_m (solid line), thermal energy E_{th} (dotted line), and kinetic energy E_k (broken line) are presented. These values are calculated by

$$E_m(t) = \int_0^1 dx \int_0^{10} \frac{B^2}{8\pi} dz, \quad (20)$$

$$E_{th}(t) = \int_0^1 dx \int_0^{10} \frac{P}{\gamma - 1} dz, \quad (21)$$

and

$$E_k(t) = \int_0^1 dx \int_0^{10} \frac{1}{2} \rho v^2 dz. \quad (22)$$

Figures 2a and 2b tell us some important features of this evolution. Figure 2a suggests that the evolution first enters on the linear stage characterized by the maximum growth rate predicted by the linear analysis. After the linear stage, we find that the growth rate slows down; this is known as one of the most important features in the nonlinear stage of tearing process, that is, an exponential growth in the linear stage is reduced or even replaced by an algebraic one in some cases (Rutherford 1973; Steinolfson & van Hoven 1984). According to Steinolfson & van Hoven (1984), if the length of current sheet is sufficiently larger than its thickness, the nonlinear evolution does not show an algebraic growth but an exponential one whose growth rate is lower than the previous one. This is confirmed in our case. The same authors also pointed out that another feature of the nonlinear stage is that the released magnetic energy is mainly converted into the thermal energy, which is consistent with our result shown in Figure 2b.

3.2. Current-Sheet Collapse in the Nonlinear Stage

The slow-down of the growth rate of resistive processes described above makes us disappointed, because it implies that we could not expect such a violent energy-release phase as is observed in real flares. The way to avoid this difficulty is to change the distribution of resistivity from a uniformly distributed resistivity to a locally enhanced one, the latter of which can cause the fast magnetic reconnection.

As a parameter representing the local enhancement of resistivity, we introduce the so-called ion-electron drift

velocity, which, in our formulation, is defined as

$$v_d \equiv \frac{|j_y|}{\rho}, \quad (23)$$

where j_y is the y -component of current density ($\mathbf{j} = \nabla \times \mathbf{B}$) and we call this the perpendicular current density hereafter. When the drift velocity is sufficiently large, the effect of particle-wave interactions becomes more dominant than that of particle-particle collisions. This means that the resistivity is strongly enhanced over the normal value based on particle-particle collisions, which is known as the anomalous resistivity (see Treumann & Baumjohann 1997). We therefore pay attention to the temporal and spatial variations of drift velocity in order to investigate whether the anomalous resistivity can occur or not.

As for the standard case ($\beta = 0.15$, $R_m = 1000$), Figure 3 displays how the spatial distribution of drift velocity varies with time. In this figure, contour lines and arrows indicate the magnetic field lines and velocity field projected onto the (x, z) -plane. A gray-scale map represents the value of drift velocity. A displayed area is $(-1, 0) \leq (x, z) \leq (1, 10)$.

By looking at Figure 3, we find that the coalescence process between those magnetic islands formed in the linear stage proceeds during the nonlinear stage. Schumacher & Kliem (1996) pointed out that the Joule heating is a dominant factor in this process. It is also found that there appear the regions where the drift velocity has a large value. Such regions are found around the so-called X-points, located around $(x, z) = (4.1, 0)$ and $(7.5, 0)$ at $t = 9$ and around $(x, z) = (4.1, 0)$ and $(8.5, 0)$ at $t = 12$.

Figure 4 is a schematic illustration of the physical situation around an X-point. Through the linear stage of tearing process, several X-points are formed in the current sheet. This figure shows that the current-sheet collapse occurs in an X-point, where the thickness of the sheet is reduced strongly. This collapse is caused by the effective outflows from X-points, which carry away a sufficient amount of perpendicular magnetic fields (y -component of magnetic fields). The thinning effect of this collapse is eventually balanced by the diffusive effect and the sheet reaches another steady state, which is suggested by Figure 5. This figure shows the time variations of drift velocity (solid line), the absolute value of perpendicular current density (dotted line), and gas density (broken line) in the standard case ($\beta = 0.15$ and $R_m = 1000$), all of which are averaged over the range of $(0, 3.72) \leq (x, z) \leq (0, 4.52)$ which corresponds to the position of the collapsed sheet (see Fig. 3). In Figure 5, it is found that there are three different stages in the temporal development of current-sheet collapse. In the first stage, both the drift velocity and the absolute value of the current density gradually decrease with time because currents are dissipated under a uniformly distributed resistivity. After that, they begin to increase rapidly, which reflects the dynamical collapse of the sheet. Finally, such enhancements of these physical variables finish and all these physical variables are kept constant, which suggests that the sheet reaches another steady state. Here, using the Sweet-Parker model of the current sheet, we then investigate the physical situation of this steady state. If we assume that the length of the collapsed sheet is nearly equal to the wavelength of the most unstable tearing mode, that length is expressed as

$$\lambda/L \sim 4.9R_m^{1/4}(\gamma\beta)^{-1/8}(l/L)^{5/4}, \quad (24)$$

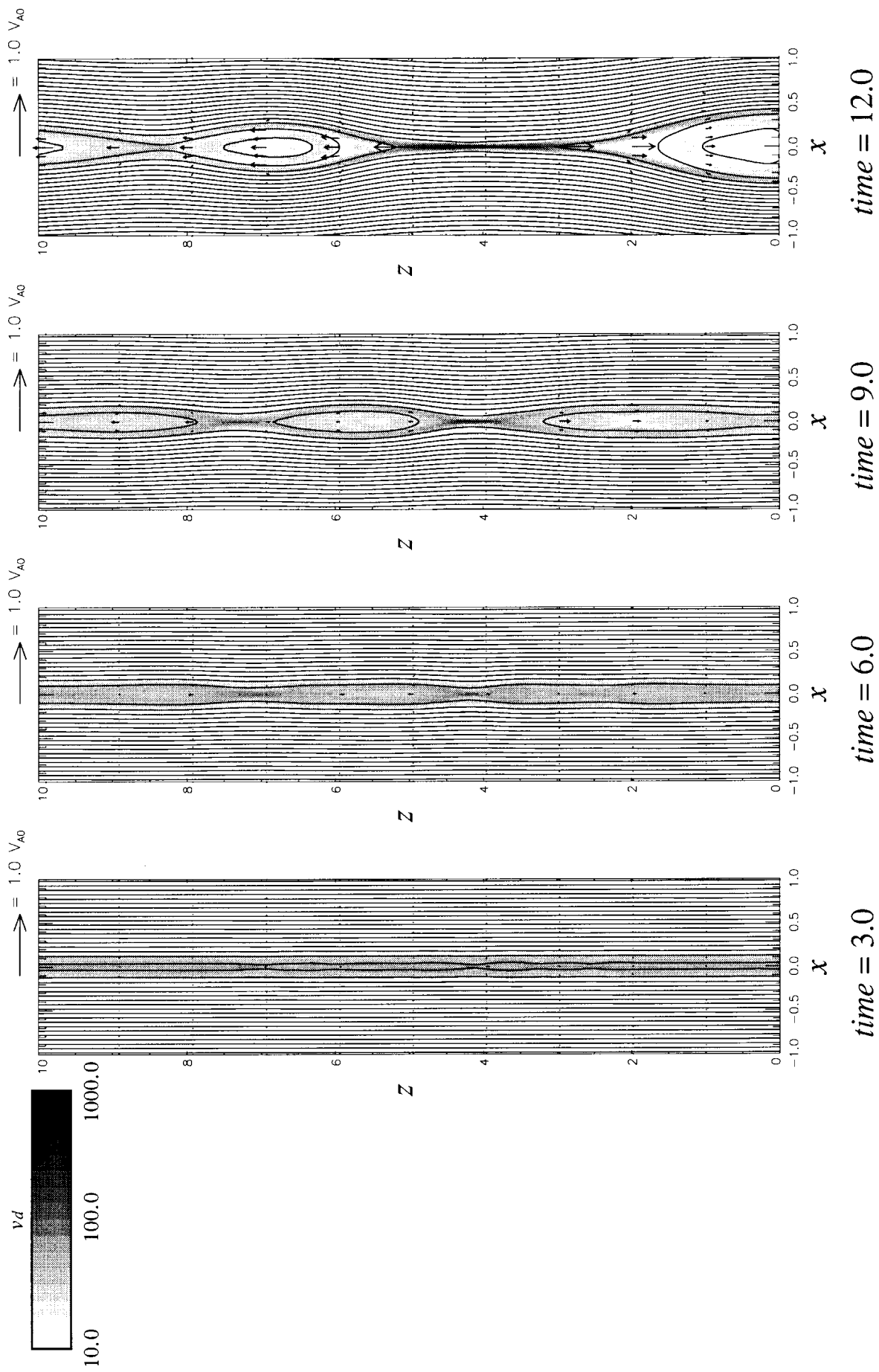


FIG. 3.—Evolution of the standard case ($\beta = 0.15$ and $R_m = 1000$). Contour lines, arrows, and a gray-scale map represent the magnetic field lines, velocity field, and the value of drift velocity projected onto the (x, z) -plane. Elapsed times are $t = 3, 6, 9,$ and 12 from left to right.

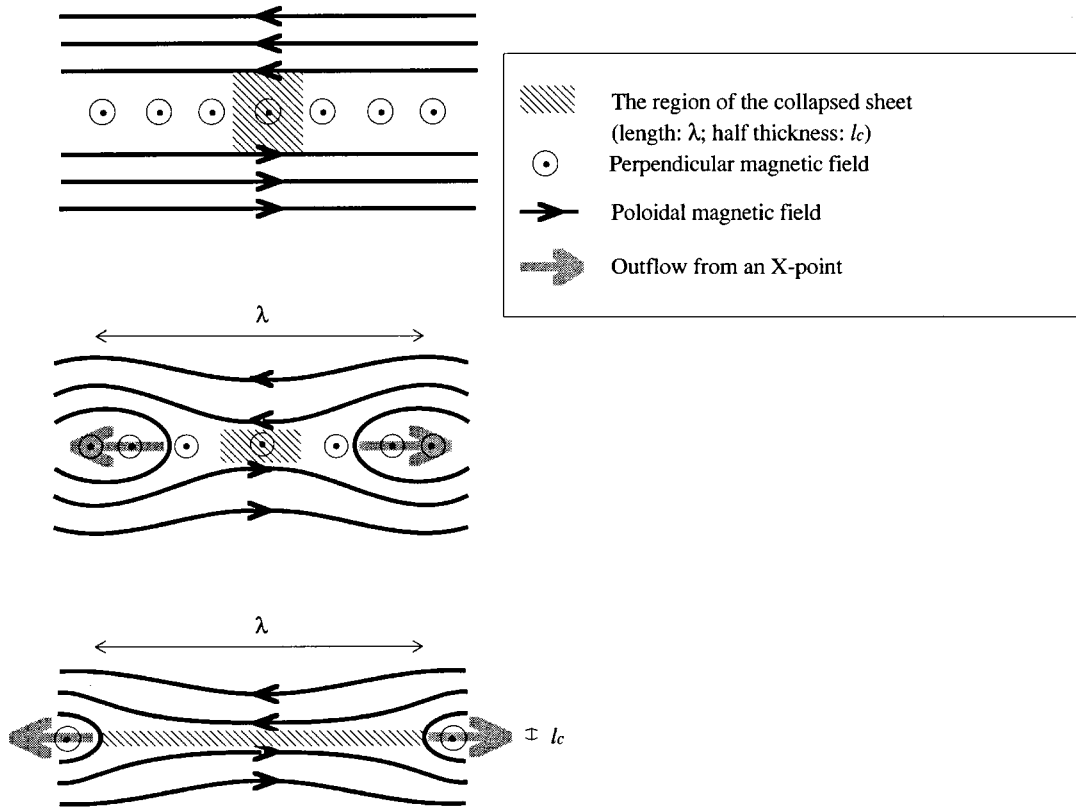


FIG. 4.—Schematic illustration of *current-sheet collapse* caused by the effective outflows carrying a sufficient amount of perpendicular magnetic fields away from an X-point. λ is the wavelength of the most unstable tearing mode, which is considered to be nearly equal to the length of the collapsed sheet; l_c is a half thickness of this sheet.

where $R_m \equiv c_s L/\eta$, l is an initial half-thickness of the sheet, and L is a unit length (see, for example, Sturrock 1994). For the standard case [$\beta = 0.15$, $R_m = 1000$, $l/L = (4\pi)^{-1}$], equation (24) gives us $\lambda/L \sim 1.4$. When we see the panel of $t = 12$ in Figure 3, we can find that this value is approximately equal to the length of the collapsed sheet. (Actually, this length becomes large with time so that its value [about two in the panels of $t = 12$ in Fig. 3] is slightly larger than the wavelength of the most unstable tearing mode [about 1.4 derived from eq. (24)].) Next, we evaluate the thickness

of the collapsed sheet and the inflow velocity. Once the Sweet-Parker model is established in the collapse sheet, the half-thickness of this sheet (l_c) and the inflow velocity toward the sheet (v_{inflow}) are expressed as

$$l_c = (\lambda/2)/R_{m,S-P}^{1/2}, \tag{25}$$

and

$$v_{\text{inflow}} = v_A/R_{m,S-P}^{1/2}, \tag{26}$$

where $R_{m,S-P} \equiv (\lambda/2)v_A/\eta$ (see Parker 1994). In our formulation, these values are evaluated in the following way:

$$l_c/L \sim 1.3R_m^{-3/8}(\gamma\beta)^{3/16}(l/L)^{5/8}, \tag{27}$$

and

$$v_{\text{inflow}}/c_s \sim 0.8R_m^{-5/8}(\gamma\beta)^{-3/16}(l/L)^{-5/8}. \tag{28}$$

Then we check the validity of these formulae by using the standard case ($\beta = 0.15$, $R_m = 1000$). Figure 6 indicates the horizontal distributions of perpendicular current density (solid line) and inflow velocity (dotted line). An elapsed time is 12, and both distributions are averaged over the range of $3.72 \leq z \leq 4.52$, which corresponds to the position of the collapsed sheet. We also depict the initial distribution of perpendicular current density in this figure, represented by a broken line. In this case, equations (27) and (28) give $l_c/L \sim 0.02$ and $v_{\text{inflow}}/c_s \sim 0.06$ with $R_m = 1000$, $\gamma = 5/3$, $\beta = 0.15$, and $l/L = (4\pi)^{-1}$. Compared with these results, Figure 6 shows that the half-thickness of the collapsed sheet

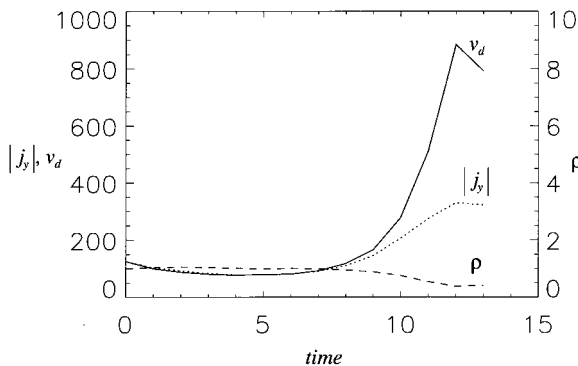


FIG. 5.—Time variations of drift velocity (solid line), the absolute value of perpendicular current density (dotted line), and gas density (broken line) in the standard case ($\beta = 0.15$ and $R_m = 1000$), all of which are averaged over the range of $(0, 3.72) \leq (x, z) \leq (0, 4.52)$ which corresponds to the position of the collapsed sheet (see Fig. 3).

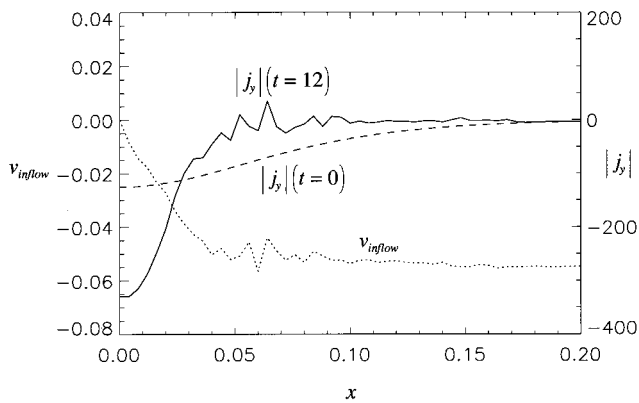


FIG. 6.—Horizontal distributions of perpendicular current density (solid line) and inflow velocity (dotted line). An elapsed time is 12 and both distributions are averaged over the range of $3.72 \leq z \leq 4.52$. A broken line shows the initial distribution of perpendicular current density. The negative value of inflow velocity means that a plasma flows into the current sheet.

is about 0.03 and the inflow velocity is about 0.05. These results suggest that the above formulae based on the Sweet-Parker model describe the dynamical collapse fairly well. We also checked the cases in which we changed the values of magnetic Reynolds number and plasma beta and confirmed that these formulae had a reasonable validity in those cases.

Next, we present the results on the timescale of the dynamical collapse. Figures 7a and 7b show the time variations of the enhancement of perpendicular current density under several values of magnetic Reynolds number and plasma beta, respectively. The current density is averaged over the part of the z-axis which corresponds to the position of the collapsed sheet. These figures clearly show that the collapse in the nonlinear stage proceeds rapidly when the magnetic Reynolds number is large and the plasma beta is low. We think that this is because a weak diffusive effect is made on the external magnetic fields when the magnetic Reynolds number is large. Therefore, there can exist a strong external magnetic force in that case and this force gives rise to strong inflows, which is clearly confirmed in Figures 8a–8c. These figures show the temporal development of inflow velocity in the cases of $R_m = 1000$ and 1500. Here the inflow velocity is averaged over the part of the z-axis which corresponds to the position of the collapsed

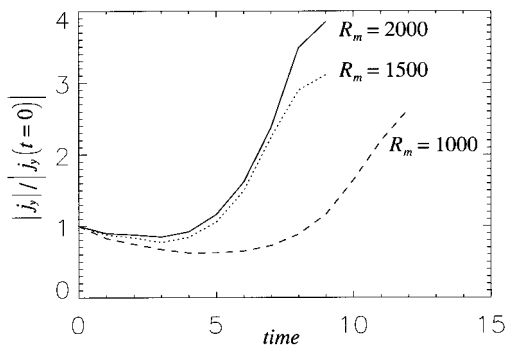


FIG. 7a

sheet. A dotted line and a dashed line represent the cases of $R_m = 1500$ and 1000, respectively. Elapsed times are $t = 1$ (linear stage), $t = 4$, and $t = 7$ for Figures 8a, 8b, and 8c, respectively. From these figures, it is found that there is little discrepancy between the two cases in the linear stage (see Fig. 8a), while the case of larger magnetic Reynolds number is found to have a stronger inflow in the nonlinear stage (see Figs. 8b and 8c). According to Fu & Lee (1986), the growth rate of current density in the current sheet is expressed as

$$i\omega \sim \frac{2}{\delta} \left(v_{\text{inflow}} - \frac{\eta}{\delta} \right), \quad (29)$$

where $i\omega$ is a growth rate and δ is a half-thickness of the sheet. Equation (29) also implies that the rapid enhancement of current density occurs when the magnetic Reynolds number is large (small resistivity) and the inflow is strong. As for the effect of plasma beta, a similar argument can be made, that is, when the plasma beta is low, the inflow becomes strong because the external magnetic fields are relatively strong in that case (see Fig. 7b).

It may be worth considering, in passing, how the current-sheet collapse proceeds in those current sheets of no perpendicular magnetic fields, where the initial force balance is maintained by the enhancement of gas pressure inside the sheet instead of the pressure of perpendicular magnetic fields. The initial gas density is uniformly distributed so that the temperature is enhanced inside the sheet. We call this case the enhanced gas-pressure case and compare it to the case of perpendicular magnetic fields (force-free case). Figure 9a shows the time variation of the logarithmic increment of reconnected magnetic flux, represented by a dotted line (force-free case) and a solid line (enhanced gas-pressure case). This figure clearly shows that the nonlinear “slow-down” of magnetic reconnection begins earlier in the enhanced gas-pressure case. Another interesting point is found in Figure 9b in which the time variation of the absolute value of perpendicular current density is presented. Here a dotted line and a solid line are the force-free case and the enhanced gas-pressure case, respectively. The current density is averaged over the part of the z-axis which corresponds to the position of the collapsed sheet. Both cases in this figure qualitatively have similar evolutions, although they are different in the timescale of current-sheet collapse, that is, the collapse proceeds faster in the force-free case than in the enhanced gas-pressure case. This implies that the transition from a relatively gentle energy-release phase

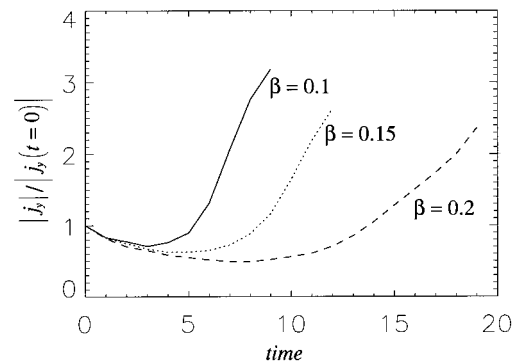


FIG. 7b

FIG. 7.—(a) Time variation of the enhancement of perpendicular current density under several values of magnetic Reynolds number; $R_m = 2000$ (solid line), 1500 (dotted line), and 1000 (broken line). The current density is averaged over the part of the z-axis which corresponds to the position of the collapsed sheet. (b) Time variation of the enhancement of perpendicular current density under several values of plasma beta; $\beta = 0.1$ (solid line), 0.15 (dotted line), and 0.2 (broken line). The current density is averaged over the part of the z-axis which corresponds to the position of the collapsed sheet.

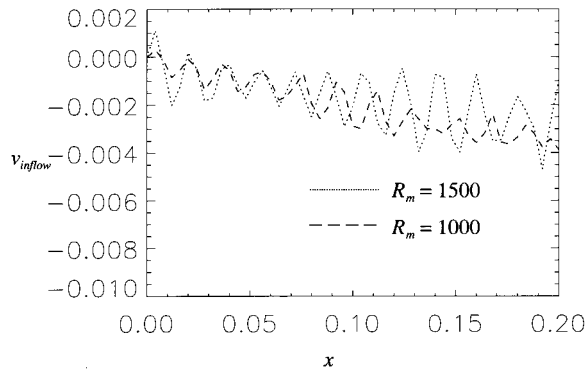


FIG. 8a

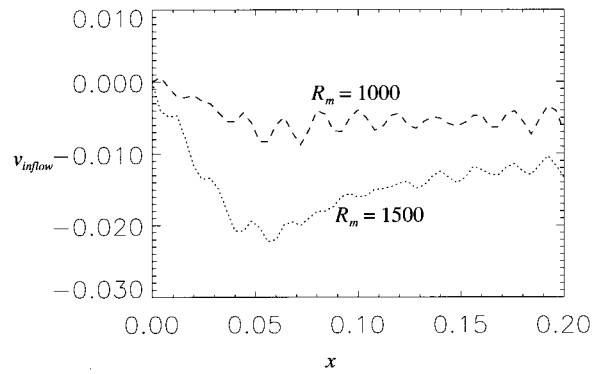


FIG. 8b

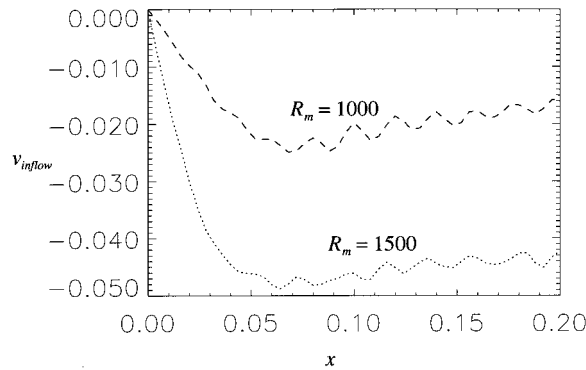


FIG. 8c

FIG. 8.—(a) Horizontal distribution of inflow velocity in the cases of $R_m = 1000$ and 1500 . An elapsed time is $t = 1$. The negative value of inflow velocity means that a plasma flows toward current sheet. (b) Elapsed time of $t = 4$. (c) Elapsed time of $t = 7$.

to the violent energy-release phase occurs more rapidly in the force-free case than in the enhanced gas-pressure case, which can be roughly understood in the following way. In the enhanced gas-pressure case, a high-pressure gas always fills the current sheet to resist the rapid collapse of sheet. In the force-free case, on the other hand, once perpendicular magnetic fields are ejected out of the current sheet, there is neither high-pressure hot gas nor perpendicular magnetic fields in it so the sheet can collapse freely until the gas pressure in the sheet is enhanced strongly enough to balance the external magnetic pressure. We will do more detailed study on this topic in our future work.

4. FAST MAGNETIC RECONNECTION TRIGGERED BY THE OCCURRENCE OF ANOMALOUS RESISTIVITY

In this section, we discuss how the system can evolve to the stage of fast magnetic reconnection, which causes the violent energy release. First of all, we cast our attention to the time variations of the intensities of several kinds of radiation observed in solar flares. Figure 10 shows a schematic illustration of them, associated with the names of observational phases. This figure tells us some important features of the flare evolution. For soft X-rays and EUVs, it is found that their intensities begin to increase in the preflare phase.

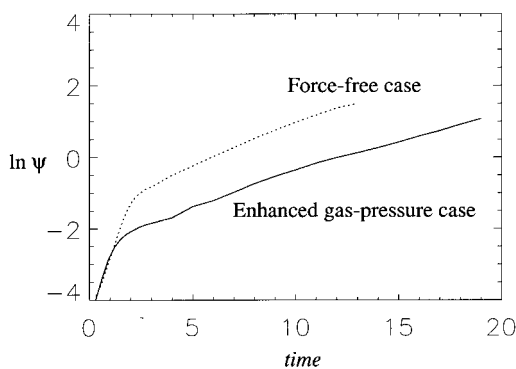


FIG. 9a

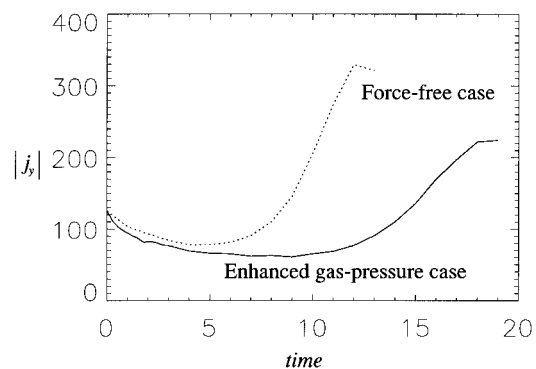
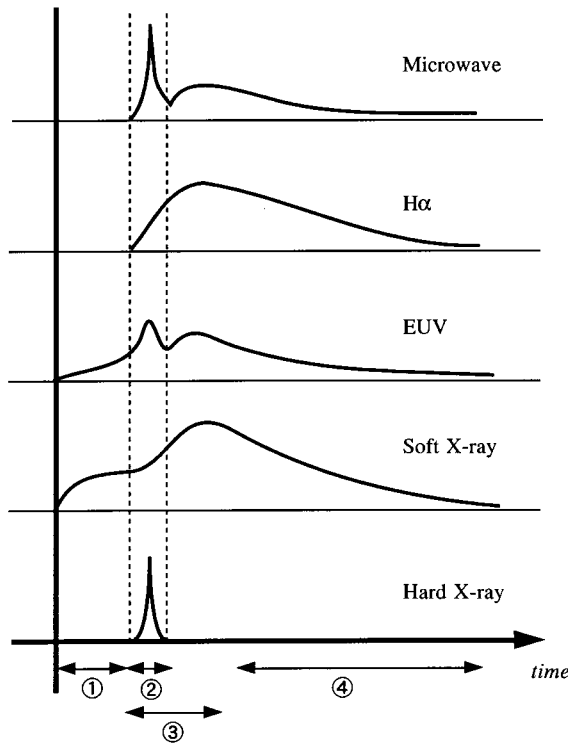


FIG. 9b

FIG. 9.—(a) Time variation of the logarithmic increment of reconnected magnetic flux, represented by a dotted line (force-free case) and a solid line (enhanced gas-pressure case). (b) Time variation of the absolute value of perpendicular current density, represented by a dotted line (force-free case) and a solid line (enhanced gas-pressure case).



Observational phases

- ① Preflare phase
- ② Impulsive phase
- ③ Rise phase
- ④ Gradual phase

FIG. 10.—Schematic illustration of the time variations of the intensities of several kinds of radiation observed in solar flares, associated with the names of observational phases.

After reaching a critical point, they are abruptly enhanced and at the same time the pulslike behaviors of hard X-rays and microwaves are observed. These features imply that a significant energy release occurs even in the preflare phase and that energy release is dramatically enhanced when going over a critical point.

Then we try to explain these observational features by using the results obtained in this study. Here, one important point we should notice is the existence of the preflare heating, which suggests that not ideal MHD but resistive MHD processes work in the preflare phase. (In this respect, it may be possible to consider any ideal MHD process causing the adiabatic heating, although we do not discuss this process here. The study of this topic is left to our future work.) In § 3.1 we make some investigations on the growth rate and energetics of the tearing process. The initially stored magnetic energy is mainly converted into the thermal energy during the linear and nonlinear stages, and the amount of the produced thermal energy is quite small in the linear stage compared to that in the nonlinear stage (Fig. 2*b* shows that the amount of the produced thermal energy in the linear stage is at most 10%–20% of that in the nonlinear stage). From this consideration, we infer that the nonlinear stage of tearing process mainly contributes to the preflare heating.

The next topic, which is the most important subject of this paper, is to find out how the dramatic change of the rate of energy conversions occurs when going over a critical point. Rapid energy conversions are caused by the fast magnetic reconnection, and one of the crucial factors in the fast magnetic reconnection is the anomalous resistivity, which can arise locally in very thin current sheets. Accordingly, in order to seek the cause of such change of the rate of energy conversions, we have to consider how an extremely thin current sheet can be formed naturally through the interaction among several physical processes of the flare evolution. The results presented in § 3.2 suggest that the current-sheet collapse occurs in the so-called X-points inside the current sheet and that the collapsed sheet eventually reaches another steady state described on the basis of the Sweet-Parker model. According to equations (24), (27), and (28), we then try to consider how such collapse works in the real circumstances of the corona. In this study, we take a unit length as $L = 100$ km, so that the length scale of typical large flares is about $10^3 L$. As for the magnetic Reynolds number and the plasma beta in the corona, we set $c_s L/\eta \sim (10^5 \text{ m s}^{-1})(10^5 \text{ m})/(1 \text{ m}^2 \text{ s}^{-1}) = 10^{10}$ for the former and 0.01 for the latter. In this case, the length and the half-thickness of the collapsed sheet are given by equations (24) and (27) as follows:

$$\lambda/L \sim 4.9 R_m^{1/4} (\gamma\beta)^{-1/8} (l/L)^{5/4} \sim 100, \quad (30)$$

$$l_c/L \sim 1.3 R_m^{-3/8} (\gamma\beta)^{3/16} (l/L)^{5/8} \sim 2 \times 10^{-5}. \quad (31)$$

Here we set $\gamma = 5/3$ and $l/L = (4\pi)^{-1}$. Let us assume that an MHD current sheet of macroscopic size whose length is equal to a half-length of flares, that is, $5 \times 10^2 L$, is initially formed within a magnetic arcade through some ideal MHD processes (see Mikic et al. 1988; Biskamp & Welter 1989; Finn et al. 1992; Inhester et al. 1992; Kusano et al. 1994; Choe & Lee 1996; Amari et al. 1996). Then equation (30) suggests that there appear about five X-points inside the sheet (see Fig. 11). The region near these X-points is subject to the dynamical collapse so that the thickness of the sheet around such points becomes $l_c \sim 2 \times 10^{-5} L = 2 \times 10^{-5} \times (100 \text{ km}) \sim 2 \text{ m}$. Since the initial thickness is $l \sim (4\pi)^{-1} L = (4\pi)^{-1} \times 10^2 \text{ km} \sim 10 \text{ km}$, the thickness of the sheet is reduced about 10^4 times owing to that collapse. This value lies in the range of microscopic values, that is, it satisfies the condition for the occurrence of anomalous resistivity in the corona (see § 2.3). Accordingly, we can expect that the anomalous resistivity occurs in those X-points formed inside the current sheet. Moreover, we think that such situation may be reflected by some observational facts. Taking a careful look at the time variation of hard X-ray intensity, we often find multiple enhancements in it. Since the energetic electrons producing hard X-ray emissions are considered to be generated in those regions where the resistivity is locally enhanced, such multiple enhancements in the hard X-ray intensity may be due to the frequent occurrence of the anomalous resistivity in the current sheet. This supports the idea that there appear multiple X-points inside the current sheet, in each of which the anomalous resistivity occurs. As to the inflow toward an X-point, its velocity is expressed as

$$v_{\text{inflow}} \sim 0.8 R_m^{-5/8} (\gamma\beta)^{-3/16} (l/L)^{-5/8} c_s \sim 0.4 \text{ m s}^{-1}, \quad (32)$$

when we take $R_m = 10^{10}$, $\gamma = 5/3$, $\beta = 0.01$, $l/L = (4\pi)^{-1}$, and $c_s = 10^5 \text{ m s}^{-1}$ in equation (28). This value is extremely

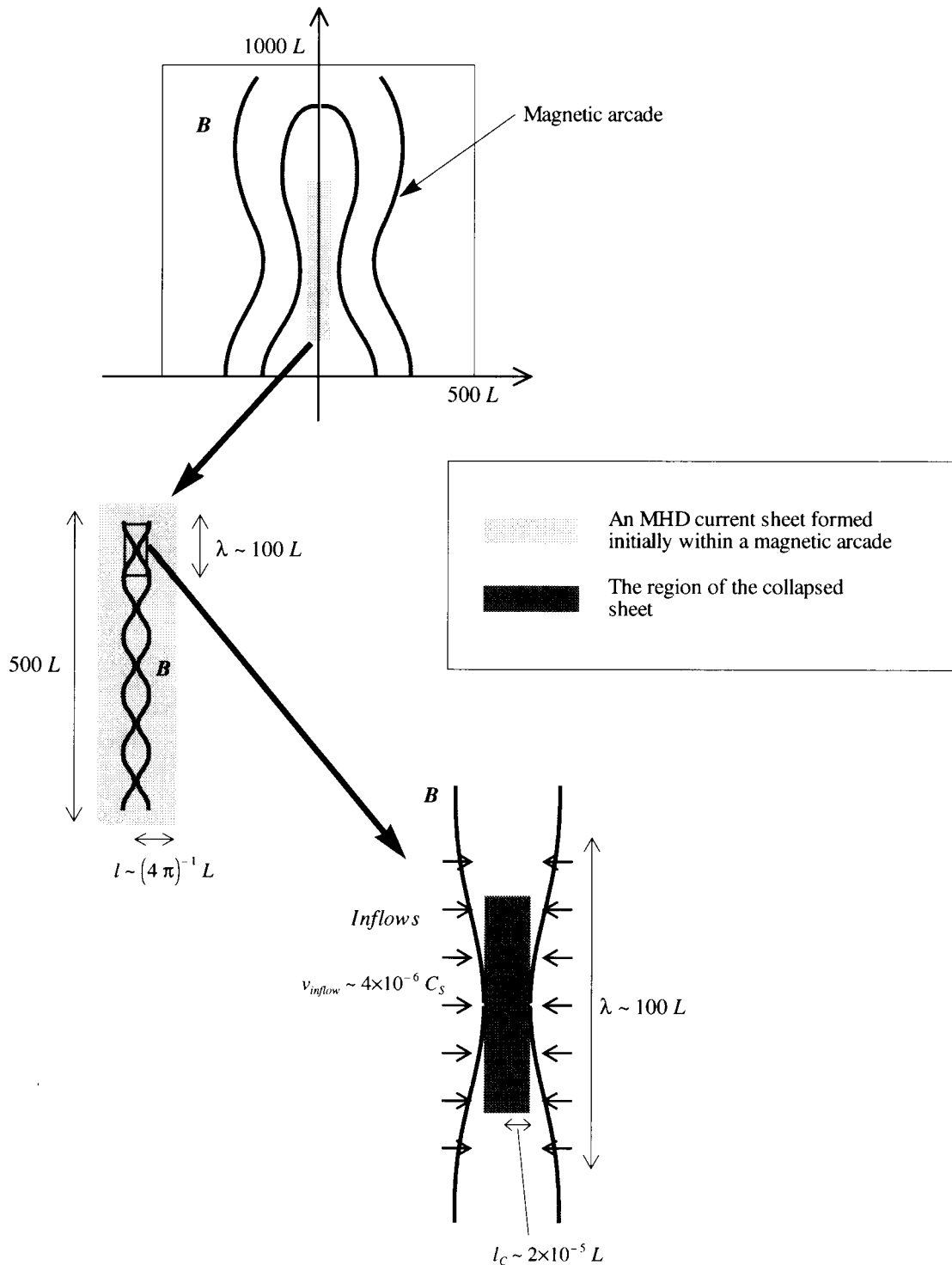


FIG. 11.—Schematic illustration of how the dynamical collapse of the sheet works in the real circumstances of the corona. For details, see text.

small, but if the resistivity is enhanced about 10^5 times and the inflow velocity is also enhanced about the same amount, it becomes of the order of $4.0 \times 10^4 \text{ m s}^{-1}$, which is consistent with the result derived from the fast magnetic reconnection flare model (see Magara et al. 1996). In this respect, Treumann & Baumjohann (1997) pointed out that the effective collision frequency becomes an order of the ion plasma frequency when the ion-electron drift velocity is very much larger than the ion-acoustic velocity. In the coronal

environment, the ion-electron collisional frequency is about 10 s^{-1} ($T_e = 10^6 \text{ K}$ and $n_0 = 10^9 \text{ cm}^{-3}$), while the ion plasma frequency is about 10^6 s^{-1} , so that the effectiveness of resistivity is enhanced about 10^5 times, although the precise mechanism of the resistivity enhancement in the corona is still unknown.

We then see how the occurrence of anomalous resistivity affects the flare evolution. To do this, we perform the numerical simulation including the effect of anomalous

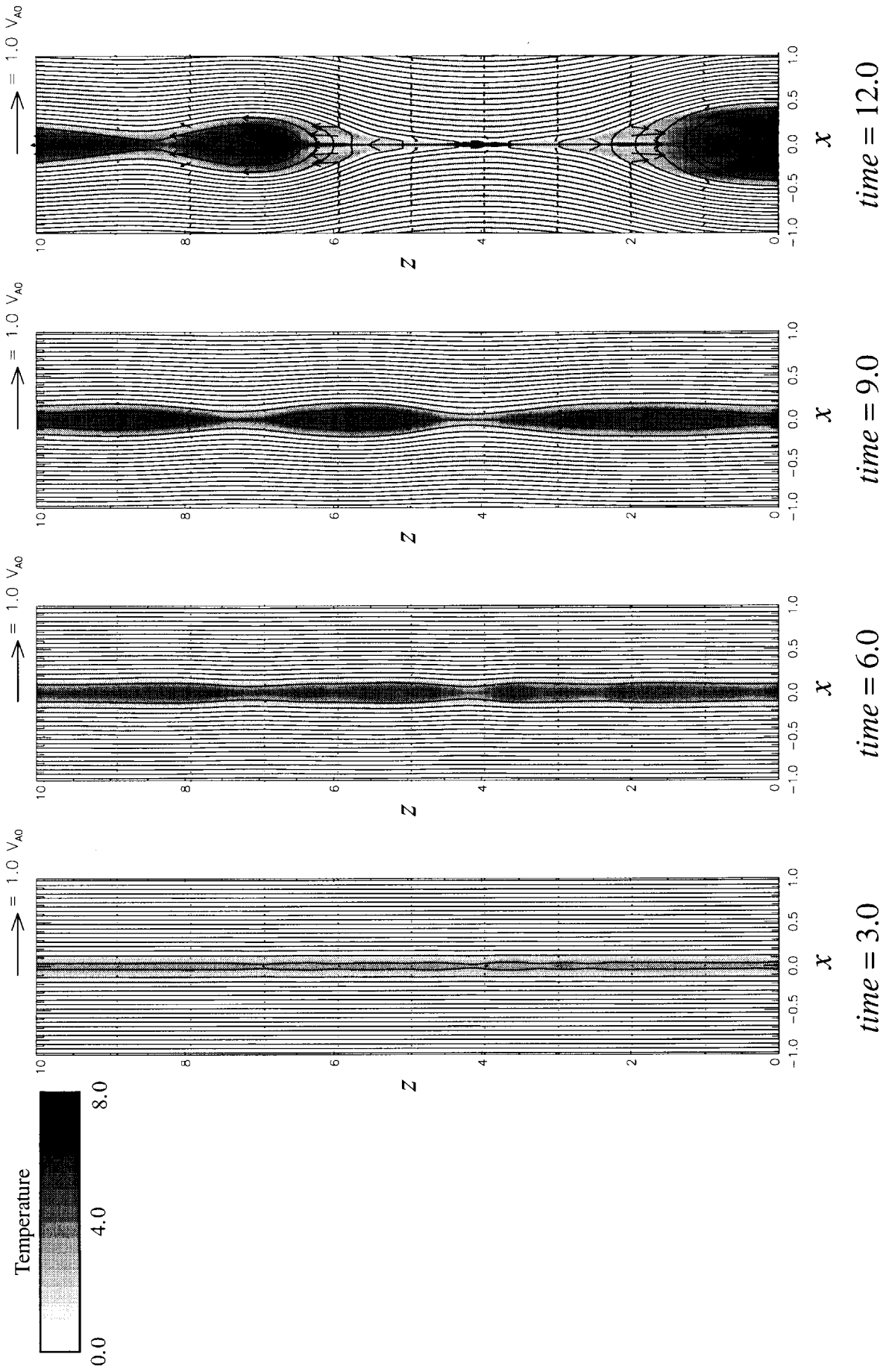


FIG. 12a

FIG. 12.—(a) Evolution of the anomalous resistivity case. Contour lines, arrows, and a gray-scale map represent the magnetic field lines, velocity field, and the value of temperature projected onto the (x, z) -plane. Elapsed times are $t = 3, 6, 9,$ and 12 from left to right. (b), (c) Includes the effect of anomalous resistivity.

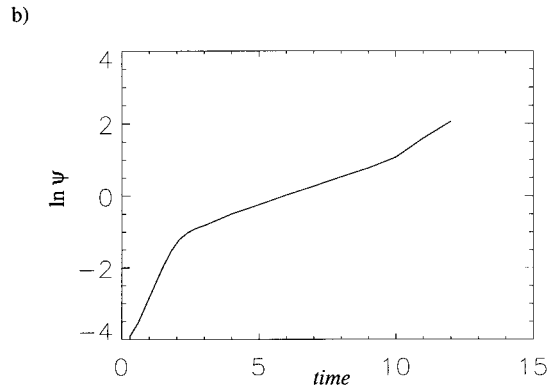


FIG. 12b

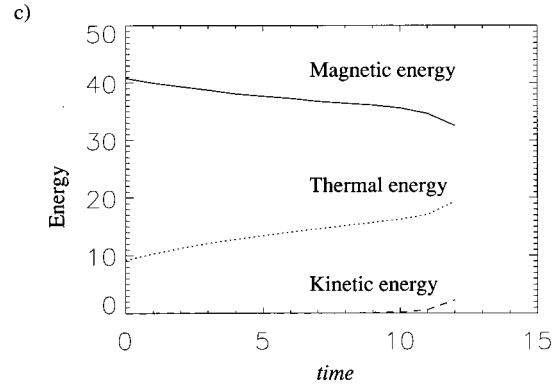


FIG. 12c

resistivity, the formula for which is given by

$$\eta = \begin{cases} 0.01 \frac{v_d}{200}, & v_d \geq 200, \\ 0.001, & v_d < 200, \end{cases} \quad (33)$$

where 200 is the critical value for the occurrence of anomalous resistivity. (The value 200 does not have a physical meaning. We take this value in order to investigate the qualitative nature of the flare evolution.) The results of this simulation are shown in Figures 12a–12c. In Figure 12a, contour lines and arrows indicate the magnetic field lines and velocity field projected onto the (x, z) -plane. The gray-scale map represents the value of the temperature. A displayed area is $(-1, 0) \leq (x, z) \leq (1, 10)$. Figures 12b and 12c are similar to Figures 2a and 2b except for the inclusion of the effect of anomalous resistivity (anomalous resistivity case) instead of a uniformly distributed resistivity (standard case). The anomalous resistivity starts at $t \sim 9$ so that both cases show similar evolutions until that time. However, after that time there appears a prominent discrepancy between the two cases. Comparing Figure 12a with Figure 3, it is found that a magnetic island of the anomalous resistivity case includes more magnetic field lines in itself than that of the standard case (see the panels of $t = 12$ in Figs. 12a and 3), which implies that the fast magnetic reconnection occurs in the anomalous resistivity case. Figure 12b also indicates the occurrence of fast magnetic reconnection by the abrupt enhancement of the amount of reconnected magnetic flux. Moreover Figure 12c shows that efficient energy conversion processes really work after $t \sim 11$. These results can allow us to explain the violent energy release observed in solar flares. Several features of this phase have been deeply studied by using the fast magnetic reconnection flare model (see Magara et al. 1996, 1997). Such previous works and Figures 12a–12c here strongly support the idea that the violent energy release in solar flares is due to the occurrence of the locally enhanced resistivity, whereby the configuration of the current sheet is changed from the Sweet-Parker type to the Petschek type. The characteristic of the Petschek type of current sheet is the occurrence of strong inflows, which can permit the fast magnetic reconnection.

5. CONCLUSIONS

On the basis of the above discussions, we can safely expect that the anomalous resistivity occurs in the coronal environment where the low- β force-free balance is main-

tained and the magnetic Reynolds number is quite large. The flare evolution starts with the formation of MHD current sheet through some ideal MHD processes, and when the timescale of such dynamical processes is longer than that of the tearing process, the flare evolution enters on the resistive stage. As for the timescale of the linear stage of the tearing process, this is given by about $(\tau_d \tau_A)^{1/2} \sim R_m^{1/2} (\gamma \beta)^{1/4} (l/L)^{3/2} \tau_S$ where $\tau_S \equiv L/c_s$. Since the coronal value of the magnetic Reynolds number is quite large, the duration of this stage becomes long. For example, we obtain $(\tau_d \tau_A)^{1/2} \sim 10^3$ s with $R_m = 10^{10}$, $\gamma = 5/3$, $\beta = 0.01$, $l/L = 1/4\pi$, and $\tau_S = L/C_s = 100$ km/100 km s $^{-1} = 1$ s. Then through the nonlinear resistive evolution, a uniform distribution of resistivity changes into a locally enhanced one. Consequently, the slow-down of the rate of energy conversions can be avoided and the evolution enters on the fast magnetic reconnection stage. One important result in this paper is that we show that several physical processes work cooperatively to change the distribution of resistivity in the flare evolution. Such processes are the tearing process, the coalescence process, and the current-sheet collapse. In this respect, Bhattacharjee, Brunel, & Tajima (1983) also discuss the importance of the coalescence process in the flare evolution. In our previous works (Magara et al. 1996, 1997), we could not investigate the preflare evolution because we started with a locally enhanced resistivity so that the situation before the resistivity is localized was out of the question in these works. In this study, we surely find out the process of the local enhancement of resistivity, which can smoothly connect with the following evolution of huge energy release discussed in our previous works. In addition, from the viewpoint of plasmoid eruption, Magara et al. (1997) suggests that the preflare phase is a quasi-static phase rather than a dynamical one, in which many small magnetic islands are probably formed by weak resistive processes and later they are merged together through the coalescence process. This is consistent with the results of the present work, in which several magnetic islands formed by the tearing instability continue to coalesce, producing a lot of thermal energy.

6. SUMMARY

Following the above considerations, we now summarize the physical processes in the flare evolution. Figure 13 is a schematic illustration of such processes and several stages, each of which is characterized by a particular physical process. In the upper part of this figure, we show the sche-

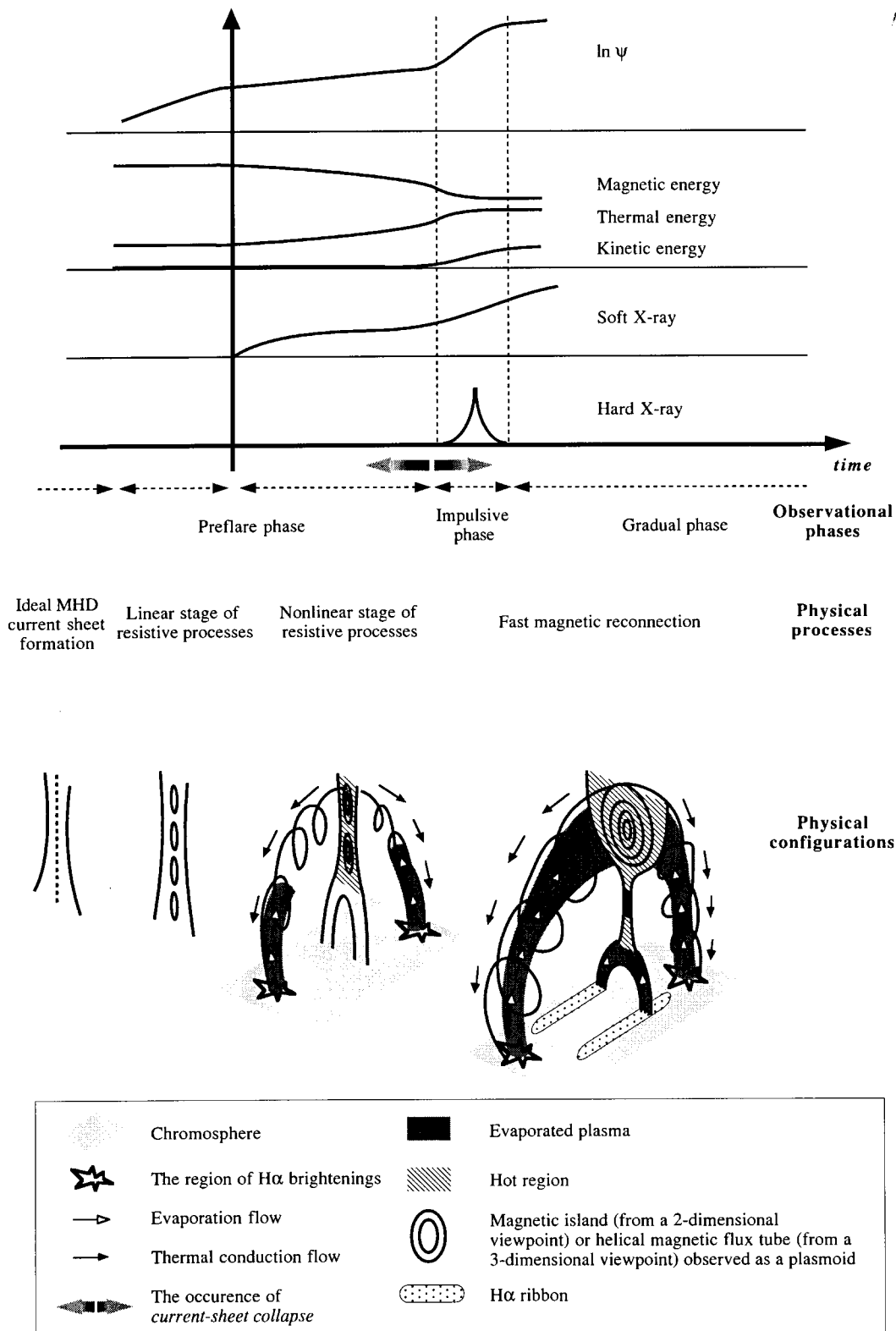


FIG. 13.—Schematic illustration of the physical processes in the flare evolution and several stages, each of which is characterized by a particular physical process. In the upper part of this figure, we show the schematic time variations of some physical values used in this paper, while physical processes are displayed in the lower part of this figure, associated with the physical configurations relevant to such processes.

matic time variations of some physical variables used in this paper, while physical processes are displayed in the lower part of this figure, associated with the physical configurations relevant to such processes. In the following, we explain the feature of every stage in the flare evolution.

6.1. Ideal MHD Current-Sheet Formation Stage

During this stage, no resistive processes work efficiently and a coronal structure makes a quasi-static ideal MHD evolution. Through that evolution, a current sheet is formed

within a magnetic arcade, which has been actually confirmed in many works (Mikic et al. 1988; Biskamp & Welter 1989; Finn et al. 1992; Inhester et al. 1992; Kusano et al. 1994; Choe & Lee 1996; Amari et al. 1996). Since this stage is dominated by macroscopic processes, the thickness of the sheet always lies in the range of macroscopic values. Before this thickness falls in the range of microscopic values, when the dynamical timescale is longer than the resistive one, resistive processes begin to work.

6.2. Linear Stage of Resistive Processes

There exists a relatively small but finite resistivity in the corona, so that any coronal structure including current sheets in itself eventually has a resistive evolution. This starts from the linear stage of tearing instability, generating many small magnetic islands in the current sheet. Since the magnetic Reynolds number in the corona is quite large, this stage usually lasts long, although the amount of the produced thermal and kinetic energies in this stage is small compared to the nonlinear stage. Consequently, this long-lasting stage is less responsible for the preflare heating.

6.3. Nonlinear Stage of Resistive Processes

In this stage, the coalescence process among those magnetic islands formed in the linear stage proceeds efficiently, producing a sufficient amount of thermal energy. Therefore, this stage corresponds to the phase in which we observe the enhancements of soft X-ray and EUV emissions, which suggests that the preflare heating occurs. Moreover, a lot of heat probably flows from hot regions in current sheet toward the chromosphere, causing H α brightenings (R. Kitai 1997, private communication) and the plasma evaporation (Ohya & Shibata 1997) in the chromosphere. The latter may contribute to the mass injection to a coronal helical loop which will later be ejected as a plasmoid.

6.4. Current-Sheet Collapse

As the nonlinear evolution proceeds, the rate of magnetic reconnection begins to slow down and energy conversions weaken. However, owing to the outflows from an X-point, this region is strongly pressed by the external force and suffer the current-sheet collapse. In a low- β and large- R_m region such as the solar corona, this collapse eventually generates a very thin current sheet, leading to the occurrence of anomalous resistivity. In this way, the transition from a uniformly distributed resistivity to a locally enhanced one is accomplished, causing the fast magnetic reconnection which enables the violent energy release.

6.5. Fast Magnetic Reconnection Stage

After the occurrence of anomalous resistivity, the rate of magnetic reconnection begins to increase and the merging among many small magnetic islands proceeds rapidly to produce a large magnetic island, or plasmoid (see Magara et al. 1997). In this stage, Petschek's configuration of the current sheet is formed macroscopically, which enables strong inflows toward an X-point. Here the fast magnetic reconnection can occur, whereby high-speed jets are produced, contributing to the acceleration of plasmoid. Since these jets effectively flow away the residual perpendicular magnetic fields around an X-point, the rate of magnetic reconnection is still more enhanced and the hard X-ray intensity also reaches its peak (see Magara et al. 1997). The heating of a plasma is now so lively that there is formed a helical loop filled with a hot plasma, which can be observed as an erupting soft X-ray plasmoid.

We mainly focus our attention on solar flares, but we think that the results presented in this paper can be also applied to other transient explosive phenomena in the Sun. That is, if such events have gradual heating as a precursor to the following main explosion, we can expect that there exist those physical processes shown above, apart from the physical scale of events.

In summary, this paper aims at understanding how the change of the energy conversion rate occurs in the flare evolution, that is, the transition from the gradual energy-release phase (preflare phase) to the violent energy-release phase (impulsive, or rise phase). We, in this study, confirm that the current-sheet collapse occurs in the flare evolution if the magnetic Reynolds number is quite large and the plasma beta is quite low. This collapse causes the occurrence of anomalous resistivity, and then the transition from a uniformly distributed resistivity to a locally enhanced one is achieved. In this way, a relatively gentle energy release in the preflare phase is replaced by the violent energy release in the impulsive or rise phase in which the fast magnetic reconnection is operating efficiently.

The authors thank T. Yokoyama for his useful discussions and also thank the anonymous referee for his instructive suggestions. The numerical computations have been carried out using NEC SX-4 at the National Institute of Fusion Science.

REFERENCES

- Amari, T., Luciani, J. F., Aly, J. J., & Tagger, M. 1996 *A&A*, 306, 913
 Bhattacharjee, A., Brunel, F., & Tajima, T. 1983, *Phys. Fluids*, 26 (11), 3332
 Biskamp, D. 1986, *Phys. Fluids*, 29, 1520
 ———. 1993, *Nonlinear Magnetohydrodynamics* (Cambridge: Cambridge Univ. Press)
 Biskamp, D., & Welter, H. 1989, *Sol. Phys.*, 120, 49
 Choe, G. S., & Lee, L. C. 1996 *ApJ*, 472, 360
 Finn, J. M., Guzdar, P. N., & Chen, J. 1992, *ApJ*, 393, 800
 Forbes, T. G., Malherbe, J. M., & Priest, E. R. 1989, *Sol. Phys.*, 120, 285
 Forbes, T. G., & Priest, E. R. 1983, *Sol. Phys.*, 84, 169
 Forbes, T. G., & Malherbe, J. M. 1991, *Sol. Phys.*, 135, 361
 Fu, Z. F., & Lee, L. C. 1986, *J. Geophys. Res.*, 91, 13373
 Furth, H. P., Killeen, J., & Rosenbluth, M. N. 1963, *Phys. Fluids*, 6, 459
 Heyvaerts, J., Priest, E. R., & Rust, D. M. 1977, *ApJ*, 216, 123
 Inhester, B., Birn, J., & Hesse, M. 1992, *Sol. Phys.*, 138, 257
 Karpen, J. T., Antiochos, S. K., & DeVore, C. R. 1996, *ApJ*, 460, L73
 Kusano, K., Suzuki, Y., Kubo, H., Miyoshi, T., & Nishikawa, K. 1994, *ApJ*, 433, 361
 Magara, T., Mineshige, S., Yokoyama, T., & Shibata, K. 1996, *ApJ*, 466, 1054
 Magara, T., Shibata, K., & Yokoyama, T. 1997, *ApJ*, 487, 437
 Mikic, Z., Barnes, D. C., & Schnack, D. D. 1988, *ApJ*, 328, 830
 Ohya, M., & Shibata, K. 1997, *PASJ*, 49, 249
 Parker, E. N. 1963, *ApJS*, 8, 177
 ———. 1994, *Spontaneous Current Sheets in Magnetic Fields* (Oxford: Oxford Univ. Press)
 Petschek, H. E. 1964, in *Proc. AAS-NASA Symp. on Solar Flares*, NASA SP-50, 425
 Priest, E. R. 1982, *Solar Magnetohydrodynamics* (Dordrecht: Reidel), 138
 Priest, E. R. 1991, *Philos. Trans. R. Soc. London A*, 336, 363
 Priest, E. R., & Forbes, T. G. 1986, *J. Geophys. Res.*, 91, 5579
 Rutherford, P. H. 1973, *Phys. Fluid*, 16, 1903
 Sato, T., & Hayashi, T. 1979, *Phys. Fluids*, 22, 1189
 Schumacher, J., & Kliem, B. 1996, *Phys. Plasmas*, 3 (12), 4703
 Shibata, K. 1997, in *Workshop on Solar Flares and Related Disturbances*, ed. T. Sakurai, E. Sagawa, & M. Akioka (Hiraiso: CRL), 36

- Shibata, K., Nozawa, S., & Matsumoto, R. 1992, PASJ, 44, 265
Shibata, K., Tajima, T., Steinolfson, R. S., & Matsumoto, R. 1989, ApJ, 345, 584
Steinolfson, R. S., & van Hoven, G. 1984, Phys. Fluids, 27 (5), 1207
Sturrock, P. A. 1994, Plasma Physics (Cambridge: Cambridge Univ. Press)
Sweet, P. A. 1958, in IAU Symp. 6, Electromagnetic Phenomena in Cosmic Physics; ed. B. Lehnert (Cambridge: Cambridge Univ. Press), 123
Treumann, R. A., & Baumjohann, W. 1997, Advanced Space Plasma Physics (London: Imperial College Press)
Ugai, M. 1994, Phys. Plasmas, 1, 2853
———. 1995, Phys. Plasmas, 2, 388
Ugai, M., & Tsuda, T. 1977, J. Plasma Phys., 17, 337
Ugai, M., & Shimizu, T. 1996, Phys. Plasmas, 3, 853
Yokoyama, T., & Shibata, K. 1996, PASJ, 48, 353